Current Applied Science and Technology e-ISSN: 2586-9396

Curr. Appl. Sci. Technol. 2025, Vol. 25 (No. 5), e0263966

Research article

Preparation of WO_3 on TiO_2 Nanotubes for Electrochromic-enhanced Photocatalytic Activity

Atsakorn Chuenkruit[1], Watcharaporn Thongjoon[1], Montri Aiempanakit[2], Chantana Aiempanakit[3] and Kamon Aiempanakit[1]*

[1]Department of Physics, Faculty of Science and Technology, Thammasat University, Pathumthani, 12121, Thailand
[2]Department of Physics, Faculty of Science, Silpakorn University, Nakhon Pathom, 73000, Thailand
[3]Division of Physics, Faculty of Science and Technology, Rajamangala University of Technology Thanyaburi, Pathumthani, 12110, Thailand

Received: 10 July 2024, Revised: 28 October 2024, Accepted: 21 November 2024, Published: 28 March 2025

Abstract

The aim of this study was to enhance photocatalytic activity through an electrochromic process. Multilayer films comprising WO_3 deposited on TiO_2 nanotubes (TNTs) were fabricated on ITO (indium tin oxide) glass substrates. The TNTs layers were synthesized via the anodization of Ti films, with variations in the deionized water content (1, 3, and 5 wt%) in ethylene glycol and NH_4F as electrolyte solutions. The results revealed that the DI water ratios during anodization significantly affected the morphological and crystalline characteristics of the TNTs. At a 3 wt% deionized water ratio, the TNTs exhibited an aligned nanotube structure and a larger crystallite size of the anatase phase. At a 5 wt% DI water ratio, degradation in both the crystalline characteristics and morphology of TNTs was observed. Furthermore, the photocatalytic performance of the TNTs and the WO_3 films deposited on the TNTs (WTNTs) samples was investigated to compare between pre-colored and colored states by examining their degradation rates of methylene blue solution under 300 μW/cm^2 ultraviolet irradiation. The results of the colored states analysis indicated that the WO_3 layer enhanced color efficiency by increasing absorption, resulting in the generation of more electron-hole pairs. Consequently, this state exhibited a significantly higher degradation rate compared to the pre-colored state.

Keywords: TiO_2; WO_3; electrochromic; photocatalytic activity; anodization

1. Introduction

In recent years, titanium dioxide (TiO_2) has become highly popular for decomposing organic pollutants through its photocatalytic activity (PA) under UV irradiance (Dell'Edera et al., 2021; Padmanabhan et al., 2021), an activity that can be applied in self-cleaning glass (Garlisi et al., 2021). However, a limitation of TiO_2 is its bulk structure, which prevents

*Corresponding author: E-mail: akamon@staff.tu.ac.th
https://doi.org/10.55003/cast.2025.263966

it from reaching its full catalytic potential (Diebold, 2003; Junbang et al., 2024). Improving TiO_2 catalyst performance is commonly achieved by increasing the surface area to allow more contact with organic pollutants by reorganizing the bulk structure into nanostructures, such as nanorods, nanowires, and nanotubes. These nanostructures have a high surface area, resulting in the generation of more e^--h^+ pairs during photogeneration and thus enhanced redox reactions to degrade pollutants. In other words, this increase significantly enhances the PA performance (Zhou et al., 2024).

In addition to issues such as wastewater and air pollution, energy problems are a significant concern facing the world today due to global warming. This causes indoor environments to become hotter, compelling residents to use air conditioning, which leads to higher expenses. To address this problem, one of the promising technologies is electrochromic (EC) smart glass (Niklasson & Granqvist, 2007). This technology prevents heat from entering buildings after a small voltage is applied. One of the key materials used in this technology is tungsten trioxide (WO_3), renowned for its excellent electrochromic properties. WO_3 undergoes color changes through the double injection of electrons and ions such as H^+, Li^+, Na^+, and K^+ (Karuppasamy& Subrahmanya, 2008; Zheng et al., 2011). This mechanism allows the material to absorb light in the visible to near infrared range, effectively blocking heat from entering the building (Wu et al., 2023).

As mentioned earlier, both TiO_2 and WO_3 rely on their active surface systems, but each has functional limitations. TiO_2, while widely used as a photocatalyst material, still faces the challenge of a high recombination rate of e^--h^+ pairs, which reduces the availability of charge carriers for redox reactions and limits its overall PA efficiency. For WO_3, although it is highly effective in electrochromic applications, especially in terms of optical performance, it suffers from poor durability, which hinders long-term functionality. Additionally, its electronic band structure limits PA efficiency.

To address the problems, many researchers have explored the potential of modifying and combining TiO_2 and WO_3 to enable heterostructure functions. Smith and Zhao (Smith & Zhao, 2008) investigated a specific design to enhance photocatalytic performance in a TiO_2/WO_3 two-layer nanorod array. By combining TiO_2 with another semiconductor that has a smaller conduction band energy, such as WO_3, a charge separation effect is produced, which extends the lifetime of the e^--h^+ pairs, delays the recombination rate, and demonstrates the benefits of a two-layer system for PA performance. Meanwhile, Reyes-Gil et al. (2013) prepared WO_3 on TNTs through electrodeposition. The WO_3 on the TNT surface plays an important role in enhancing EC performance by providing a larger surface area for charge-transfer reactions, which facilitates ion diffusion. This results in increased insertion–extraction charge capacity and enhances both contrast and stability in the electrochromic process. Ultimately, the composite materials of WO_3 on TNTs demonstrated higher electrochromic performance compared to pure WO_3 and TiO_2.

At this point, the correlation between PA and EC phenomena remains a hot topic. However, we could not find any literature that mentions PA performance in the colored state via the EC process. One of the main factors influencing PA performance is the number of carriers on the surface, with higher quantities typically leading to better degradation (Alves et al., 2017; Zhang et al., 2022). The EC mechanism relies on the intercalation of electrons and ions, which increases the surface charge density of the material (Cao et al., 2010; Liu et al., 2020). After considering that, this research was aimed to study the impact of PA performance in TNTs and WTNTs before and after coloration achieved via the EC process by monitoring the degradation of methylene blue (MB) under UV irradiation to assess the effects.

We focused on preparing TNTs through anodization, an electrochemical process that oxidizes Ti in an electrolyte solution containing ethylene glycol (EG), deionized (DI) water, and ammonium fluoride (NH_4F). The anodization process promotes the formation of a nanotube film. When voltage is applied, Ti is oxidized to Ti^{4+} and reacts with O^{2-} in the electrolyte, resulting in the formation of TiO_2. Once the TiO_2 film forms, F^- in the electrolyte etches the oxide, dissolving parts of the film into $[TiF_6]^{2-}$. In regions of high electric field intensity, this etching creates pores while the oxide barrier layer grows. The interaction between etching and oxide barrier growth leads to the formation of nanotube structures, significantly increasing both the length and diameter of the tubes, thereby enhancing the surface-active area. For efficient TNT synthesis, controlling anodization parameters is essential to obtain the desired nanotube morphology. This remains challenging, and significant attention has been drawn to factors such as electrolyte concentration, electrolyte pH, anodization voltage, time, and temperature (Bae et al., 2008).

In this study, we examined the influence of electrolyte concentration. It is well recognized that, under the same conditions, different electrolytes can produce varying electric field intensities. Additionally, it is known that in the initial stage of anodization, a higher electric field intensity can induce larger sites, ultimately resulting in a wider diameter of TNTs. We aim to find the right balance between electrolyte viscosity to prevent the breakdown of TNTs during anodization while achieving a high surface area, and porosity by adjusting the ratio of DI water to facilitate better charge insertion during the EC process within the film structure (Corrente et al., 2020; Yao et al., 2024). Furthermore, a layer of W was to be deposited on top of TNTs (TNTs → WTNTs) using DC magnetron sputtering to enhance EC efficiency. Additionally, all samples underwent thermal oxidation (TO) in a furnace at 500°C for 1 h to form metal oxides. The reaction involved was $W^{6+} + 3O^{2-} \rightarrow WO_3$. The tungsten trioxide (WO_3) layer also plays a crucial role in initial light absorption, particularly low-energy light, due to its low E_g (2.8 eV), which is opportune in photogeneration (Sajan et al., 2017; El-Yazeed & Ahmed, 2019; Wahyuono et al., 2019; Ya et al., 2021; Thakur et al., 2023;), as shown in Figure 1.

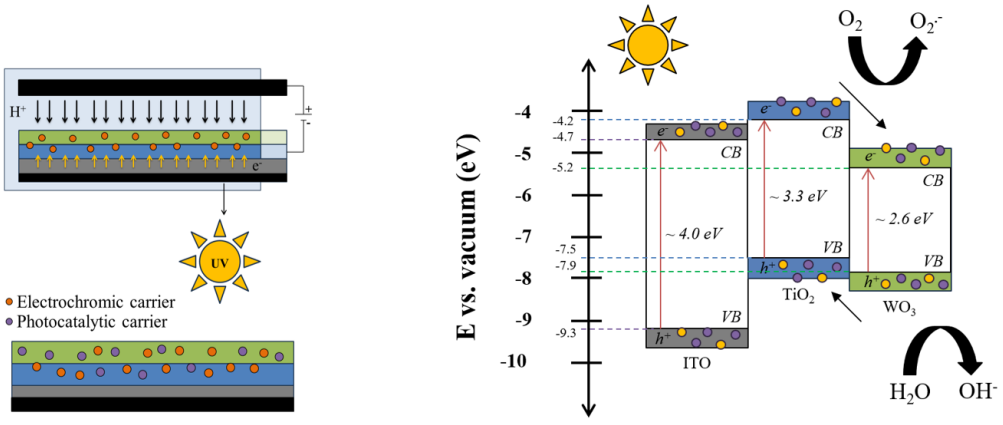

(a) (b)

Figure 1. Scheme of (a) EC and PA and (b) mechanism of the PA

2. Materials and Methods

The 100 nm thick ITO coated on glass substrates underwent cleaning using an ultrasonic process with acetone, ethanol, and DI water each for 15 min. After that, 500 nm thick metallic Ti films were deposited on the ITO glass substrate (glass/ITO/Ti) using the DC magnetron sputtering technique. A 2-inch Ti disc (99.995% purity, Kurt J. Lesker Company) was used as the target. Argon (99.999% purity) at a flow rate of 15 sccm was used as the sputtering gas in a high vacuum chamber system at a base pressure of 5.0×10^{-5} mbar using a rotary pump coupled with a diffusion pump. The sputtering power was set to 150 W. The process continued to the next step once the deposition was completed.

2.1 Preparation of TNTs

An electrolyte solution was prepared consisting of NH_4F, EG, and DI water with a total volume of 60 g. The DI water ratios were varied to 1, 3, and 5 wt% for each condition as summarized in Table 1. The Pb cathode and the glass/ITO/Ti anode were connected. The electrodes were immersed in the electrolyte as shown in Figure 2 and a constant voltage of 25 V was applied for 1 h to form TNTs. After the process, the films were cleaned using an ultrasonic cleaner with DI water for 10 min to remove any debris covering the top of the TNTs.

Table 1. Preparation of TNTs with varying DI water ratios at 1, 3, and 5 wt% in the electrolyte

Samples	Electrolyte (wt%) NH_4F + EG + DI water	NH_4F (g)	EG [1.113 g/mL] (mL)	DI water (mL)
TNTs 1%	0.60 + 98.4 + 1.0	0.36	53	0.60
TNTs 3%	0.60 + 96.4 + 3.0	0.36	52	1.8
TNTs 5%	0.60 + 94.4 + 5.0	0.36	51	3.0

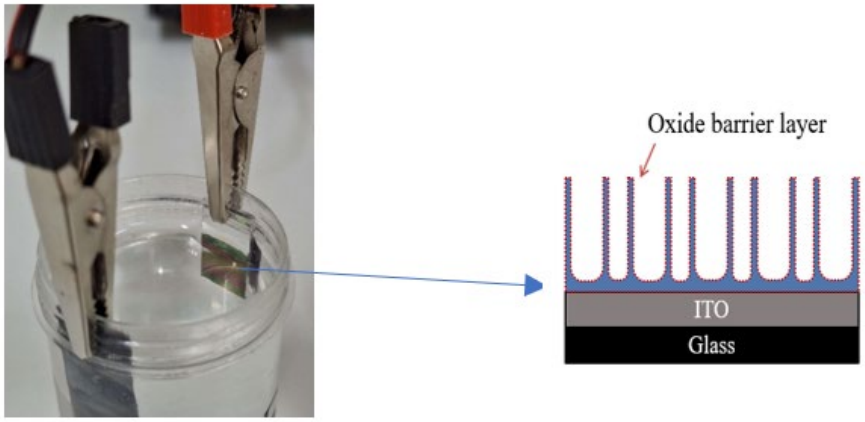

Figure 2. Experimental setup for anodization of TNTs

2.2 Preparation of WTNTs

After preparing the TNT films through the anodization process and cleaning them with an ultrasonic cleaner in DI water for 10 min, a 100 nm thin metallic W film was deposited on the TNTs using DC magnetron sputtering with a sputtering power of 100 W. A 2-inch W disc (99.95% purity, Kurt J. Lesker Company) was used as the target under the same sputtering gas, flow rate, and base pressure conditions as for glass/ITO/Ti. The scheme for preparing the WTNTs is shown in Figure 3. After preparing TNTs and WTNTs, all samples were heated to form metal oxides using the TO technique in a furnace at 500°C for 1 h.

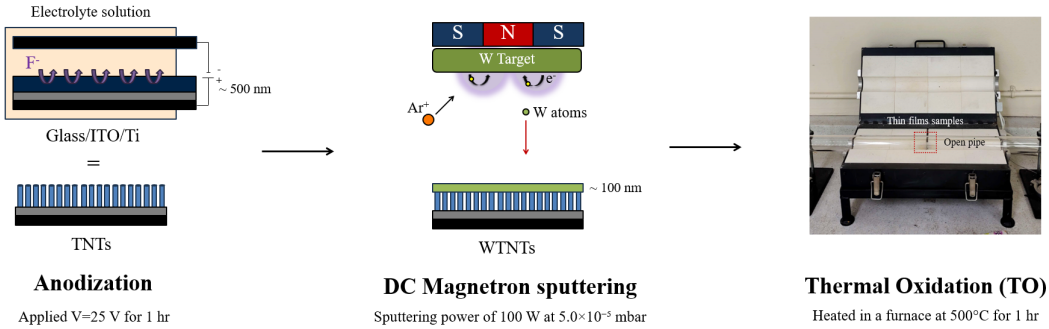

Figure 3. Experimental setup for the preparation of WTNTs samples with 3 steps (a) anodization, (b) DC magnetron sputtering, and (c) thermal oxidation

2.3 Characterization

The surface morphology of the TNT and WTNT samples after TO at 500°C for 1 h were investigated using FE-SEM (Tescan Mira 3, Czech Republic). Crystal structures were determined using XRD (D2 PHASER, Bruker) with Cu Kα radiation at 1.54 Å. A scanning range of 20°-80° and a time per step of 0.2 s with increments of 0.02° were used. The optical properties and PA performance of the TNT and WTNT samples were determined before and after coloration. In the coloration process, a DC voltage of 1.5 V was applied, with the films acting as the cathode and Pb as the anode. The samples were dipped in H_2SO_4 as the electrolyte for 1 min, and the T% at 200-1000 nm was measured using a UV-Vis spectrophotometer (Genesys S10, Thermo Scientific). The PA before and after coloration was tested by measuring the relative absorbance of MB with a base concentration of 0.025±0.005 mM as an organic pollutant under a UV lamp (Silver light 10W/T8/BL Blacklight) with irradiance of 300±20 μW/cm², recording every 50 min for 200 min.

3. Results and Discussion

3.1 Morphology

The top and cross-sectional views of the TNT and WTNT samples were observed using FE-SEM as shown in Figure 4, and the pore diameter and tube length were measured using ImageJ software, with Gaussian distribution plots shown in Figure 5 and data

summarized in Table 2. The results showed that the 1 and 3% TNTs exhibited interconnected nanotube walls, with tube length increasing after raising the DI water ratios in the electrolyte. The electrolyte concentration directly affects charge mobility during anodization, influencing the rate of etching and the formation of TNT structures (Chin et al., 2016; Suhadolnik et al., 2020; Kato & Shirai, 2022; Yu et al., 2022). A lower viscosity of the electrolyte solution enhances ion mobility in the anodization process, promoting etching and pore growth. This growth results in an increase in both the length and diameter of the tubes, with reported lengths increasing from 703.0 nm to 930.7 nm and average diameters increasing from 37.16 nm to 43.48 nm for TNTs 1 and 3%, respectively. In contrast, TNTs 5% exhibited tube deformation, resulting in the peeling of TNTs from the surface, which showed the collapse and destruction of the nanotubes, leaving only thin TiO_2 films attached to the glass/ITO. This was supported by Saharudin et al. (2018), who studied the parameters affecting morphology and found that H_2O facilitated the extraction of O_2^- and OH^- from the electrolyte to form the oxide layer, contributing to the formation of long nanotubes with thick walls. However, an excessive amount of H_2O, resulting in low viscosity, can lead to the formation of unstable nanotubes that collapse due to rapid etching effects, thereby reducing nanotube length. After considering that, the viscosity of the electrolyte significantly affects the growth and stability of TNTs during anodization. Low-viscosity electrolytes, such as those with high DI water content, can lead to faster diffusion of ions, resulting in longer nanotubes and a transition from inconsistent to uniform TNT structures. However, excessive DI water content can also cause increased destruction of the tube walls, potentially leading to structural defects, such as the breakdown of the nanotubes, especially if there is an imbalance between the oxidation and etching processes.

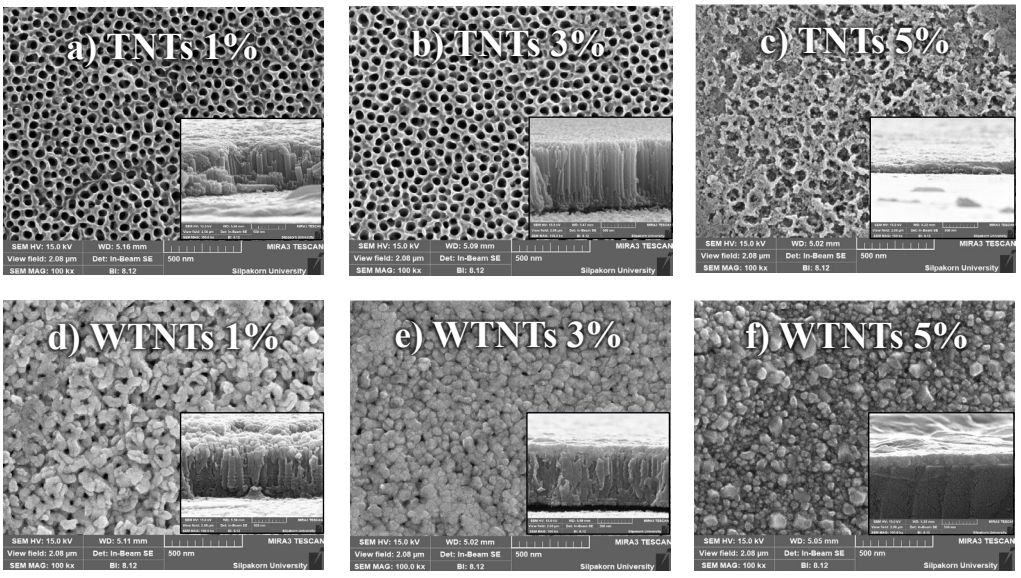

Figure 4. Top and cross-sectional views of FE-SEM images of (a) TNTs 1%, (b) TNTs 3%, (c) TNTs 5%, (d) WTNTs 1%, (e) WTNTs 3%, and (f) WTNTs 5% after TO at 500°C for 1 h

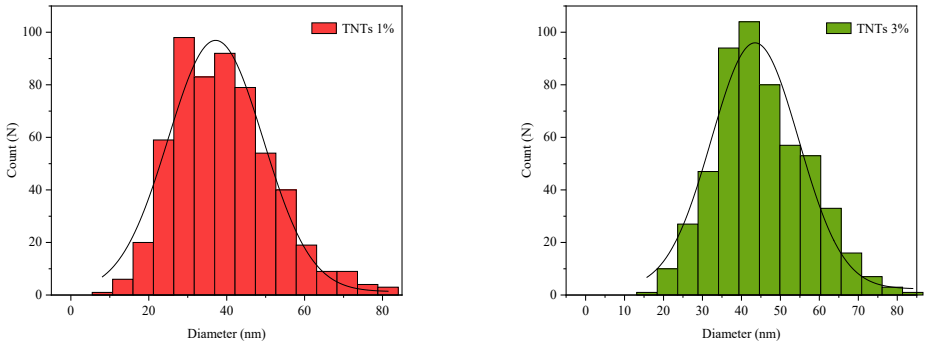

(a) (b)

Figure 5. The distribution of pore diameters of TNTs samples under DI water ratios of (a) 1 wt% and (b) 3 wt%

Table 2. The average pore diameter and tube lengths of TNT and WTNT samples

Samples	Avg Diameter (nm)	Avg Thickness (nm)
TNTs 1%	37.16±10.37	703.0±57.01
TNTs 3%	43.48±9.530	930.7±25.33
TNTs 5%	-	150.8±26.78

For the WTNTs, the 100 nm thick W film deposited on the TNTs resulted in the WO_3 layer covering the TNTs in a significantly thicker layer on top of the tubes. Varying the DI water ratios resulted in different morphological characteristics. In the WTNT 1% samples, similar to the morphology of TNTs 1%, a wide distribution of tube lengths and pore diameters was observed, resulting in a rough surface where the distribution of W atoms over the tubes created more space and greater porosity on the surface. In contrast, the WTNTs 3% showed WO_3 films with smaller grain sizes and a smoother surface, reflecting a more uniform arrangement of tubes with less distribution in length and pore sizes. The larger pore size allowed the sputtered W atoms to be inserted into the pores. However, they likely became stacked on the surface, forming a dense WO_3 layer on top. This resulted in a more compact and less porous surface compared to WTNTs 1%, as clearly seen in the FE-SEM image. For WTNTs 5%, only the WO_3 film was observed covering the substrate due to the collapse of the nanotubes. These different morphological structures directly affect the PA and EC properties due to variation of specific surface area.

3.2 Crystal structure

The crystal structure of TNTs and WTNTs after TO at 500°C for 1 h was analyzed using an X-ray diffractometer (XRD), as shown in Figure 6 and the results are summarized in Table 3. For the TNT samples, XRD peaks were observed at 25.37° and 37.92°, corresponding to the (101) and (004) planes of the anatase TiO_2 crystal phase (JCPDS

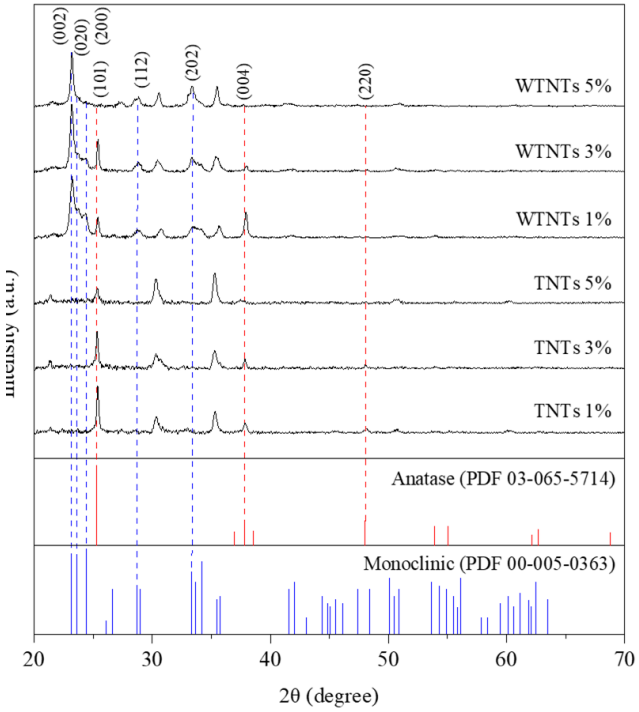

Figure 6. XRD graphs of TNTs and WTNTs after annealing at 500°C for 1 h

Table 3. Intensity and crystallite size on the (101) and (004) planes of TNTs prepared under different DI water wt%

Samples	Intensity (a.u.)		$I_{(101)}/I_{(004)}$	Crystallite size (nm)	
	$I_{(101)}$	$I_{(004)}$		(101)	(004)
TNTs 1%	11.9	3.44	3.46	59.4	33.4
TNTs 3%	9.49	3.13	3.03	60.4	32.8
TNTs 5%	4.47	1.59	2.81	37.6	8.40
WTNTs 1%	5.76	6.90	0.83	46.3	43.1
WTNTs 3%	8.77	2.54	3.45	65.2	16.2
WTNTs 5%	2.08	1.78	1.17	26.7	8.16

PDF no. 03-065-5714). For WTNTs samples, XRD peaks were observed at 23.21°, 23.77°, 24.37°, 28.83°, and 33.35° corresponding to the (002), (020), (200), (112), and (202) planes of the monoclinic WO_3 crystal phase (JCPDS PDF no. 00-005-0363). Additionally, the crystallite size was calculated using the Debye-Scherrer equation (1).

$$D = (k\lambda/\beta\cos\theta) \quad (1)$$

where D is the crystallite size, k is Scherrer's constant, λ is the X-ray wavelength (1.54 Å), and β is the full width at half maximum (FWHM) of the diffraction peak.

As mentioned earlier, increasing the DI water content while fixing the anodization time at 1 h resulted in a different arrangement of the crystal structure of TiO_2. Optimized anodization conditions supported ion diffusion, leading to increased tube length and thickness by reducing the viscosity of the electrolyte, which also enhanced the stability of the nanotube morphology during anodization by promoting crystallite growth at the (101) plane in both TNT and WTNT samples. The largest crystallite size at the (101) plane was found under the 3 wt% DI water condition due to the enhanced structural stability during the anodization process, while the smallest crystallite size occurred at the 5 wt% condition, probably due to the collapse of the tubes. For the (004) plane, the TNT samples, after DI water content increase, indicated a trend towards reduced peak intensity, with crystallite sizes significantly decreased at 33.4, 32.8, and 8.40 nm for TNTs 1, 3, and 5%, respectively.

For WTNTs, we found that increasing the DI water ratio also reduced the crystallite size at the (101) and (004) planes, which was consistent with the trend observed in TNTs. Additionally, the intensity of the $I_{(020)}$ and $I_{(200)}$ peaks from monoclinic WO_3 decreased, likely due to W atoms being inserted into the tube structure and possibly occupying oxygen vacancies with Ti atoms at the same positions. This affects the atomic arrangement and changes the crystal structure (Arvizu et al., 2014; Indira et al., 2015).

3.3 Optical properties

The TNTs and WTNTs samples after TO were classified into two states: (1) the pre-color state, represented by dashed lines, and (2) the coloration state obtained via the EC process, represented by solid lines, and hereafter referred to as C-TNTs and C-WTNTs (Figures 7 and 8). In the coloration process, a DC voltage of 1.5 V was applied to the films, with the films acting as the cathode and Pb as the anode when they were immersed in H_2SO_4 as the electrolyte for 1 min, followed by the EC process. The samples were then analyzed using a UV-Vis spectrophotometer to investigate the optical transmittance spectra (T%). Additionally, the band gap energy (E_g) of the films was determined from Tauc's plot, as shown in Figures 7 and 8.

For the TNT samples, E_g values increased from 3.41, 3.50, and 3.80 eV for TNTs 1, 3, and 5%, respectively. The TNTs 1 and 3% exhibited similar transparency, with distinct interference fringes caused by the film thickness. In contrast, TNTs 5% displayed a featureless optical response due to the severe structural collapse, as confirmed by morphological analysis. For the WTNT samples, the WO_3 deposited on TNTs resulted in reduced overall E_g values, which was consistent with W having a lower E_g of 2.6 eV. The E_g values were found to be 3.04, 3.44, and 3.83 eV for WTNTs 1, 3, and 5%, respectively. In terms of EC, the injection and extraction of H^+ ions and electron transfer between TiO_2, WO_3, and H_2SO_4 result in the EC reactions of H_xTiO_2 and H_xWO_3 (Karuppasamy, 2015), as described by equations (2) and (3).

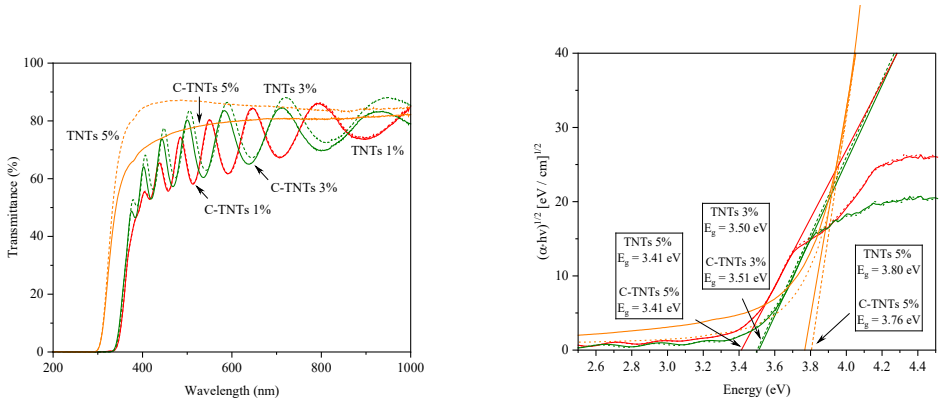

Figure 7. T% and E_g values from Tauc's plot for TNTs in before and after coloration

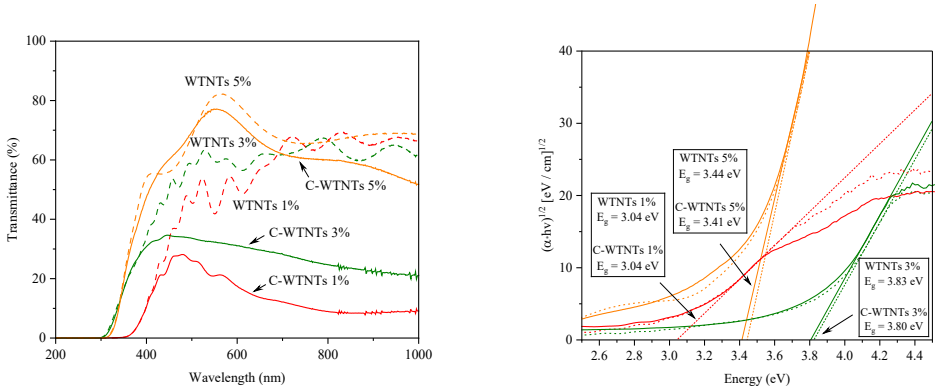

Figure 8. T% and E_g values from Tauc's plot for WTNTs in before and after coloration

$$TiO_2 + xH^+ + xe^- \text{ (pre-color)} \rightleftharpoons H_xTiO_2 \text{ (colored)} \quad (2)$$

$$WO_3 + xH^+ + xe^- \text{ (pre-color)} \rightleftharpoons H_xWO_3 \text{ (colored)} \quad (3)$$

After a specific compound forms, the color variations depend on the value of x, with a higher x value resulting in a distinct color and a lower x value corresponding to a transparent state. In the case of the C-TNTs 5%, the collapse of the tube morphology likely increased H^+ and e^- insertion, improving color formation efficiency and leading to a higher degree of coloration (Deshpande et al., 2007; Her & Chang, 2014; Huo et al., 2019; Ozkan et al., 2003). On the other hand, the C-TNTs at 1% did not show significant changes after coloration, while C-TNTs 3% exhibited only slightly coloration.

In the C-WTNTs, light absorption in the green spectrum induced a deep blue color, indicating that the W layer significantly enhanced color efficiency compared to the TNT sample. The C-WTNTs 1% exhibited a larger surface area, roughness, and porosity, which facilitate H^+ and e^- insertion due to these morphological properties. In contrast, the C-WTNTs 3% had WO_3 atoms forming a layer with a smooth and less porous surface, making it more difficult for H^+ and e^- insertion, resulting in reduced coloration efficiency compared to C-WTNTs 1% (Riyanto et al., 2023). This demonstrated that the DI water ratio also

influenced color efficiency, as it correlated with porosity and the amorphous structure. Highly disordered structures exhibited fast switching response and enhanced coloration efficiency (Fang et al., 2009; Ivanov et al., 2013; Saitow et al., 2018; Zhen et al., 2020; Thongjoon et al., 2024).

Additionally, after the EC process, we found that the E_g of both C-TNTs and C-WTNTs slightly decreased. In general, EC materials that rely on ion insertion can modify the electronic band structure, leading to bandgap widening as described by the Burstein-Moss (BM) phenomenon. This phenomenon shows that the apparent E_g of a semiconductor increases when the energy band is filled, and optical transitions must involve empty band states. This results in the absorption edge being pushed to higher energies due to certain states close to the conduction band in degenerate semiconductors, which can be expressed as: $E_{opt} = E_g + E_{BM}$, where E_{opt} is the optical band gap, E_g is the fundamental band gap, and E_{BM} is BM shift due to carrier doping. It can be concluded that the BM shift can broaden the optical band gaps following an increase in carrier density.

However, Zhou et al. (2023) reported that intercalating Li^+ ions into Y_2CF_2 at different concentrations ($Li_xY_2CF_2$ for x = ¼ and x = 1) could be employed to tune carrier density in EC devices. They found that the intercalation of small ions decreased the fundamental E_g in inorganic materials, such as transition metal oxides, which tended to counteract the BM shift. Additionally, Zhao et al. (2022) reported on the inorganic dual-band mechanism of EC in single-component WO_3 films, where the observed colors (from transparent to dark blue) depended on the varying densities of free carriers. This variation was induced by adjusting the voltage to increase double injection, resulting in a reduced E_g of the WO_3 films as the voltage was increased. This observation is relevant to our conditions for C-TNTs and C-WTNTs, as the presence of inorganic materials in the colored state may influence the optical properties and adjustments in E_g.

3.4 Photocatalytic activity

The PA performance of the TNT and WTNT samples after TO was monitored and categorized into 2 states: (i) before coloration (represented by dashed lines) and (ii) after coloration via the EC process (represented by solid lines, referred to as C-TNTs and C-WTNTs) (Figures 9 and 10). The PA performance was assessed by monitoring the degradation of MB (with an initial concentration of 0.025±0.005 mM) as an organic pollutant, under UV irradiation at 300±20 μW/cm². The relative absorbance at 664 nm was recorded every 50 min over a total duration of 200 min to determine the MB concentration. These data were plotted against time and used to calculate the degradation rate (k) based on first-order chemical kinetics (Hauch et al., 2002) as described in equation (4). The results are presented in Figures 9-11.

$$\ln\left(\frac{Co}{C}\right) = kt \quad (4)$$

where C is the MB concentration, C_0 is the initial MB concentration (0.025 mM), k is the first-order rate constant, and t is time.

The PA results of TNTs 1 and 3% (pre-color) exhibited similar k values, attributed to their comparable morphology and crystallite size, while TNTs 5% showed a lower k value due to the collapse of the tube structure, as mentioned before. After coloration by the EC process, C-TNTs 1% showed a slight increase in the k value from 0.00176 to 0.00185 m^{-1}, whereas C-TNTs 3% decreased from 0.00167 to 0.00122 m^{-1} and C-TNTs 5% slightly decreased from 0.00067 to 0.00060 m^{-1}.

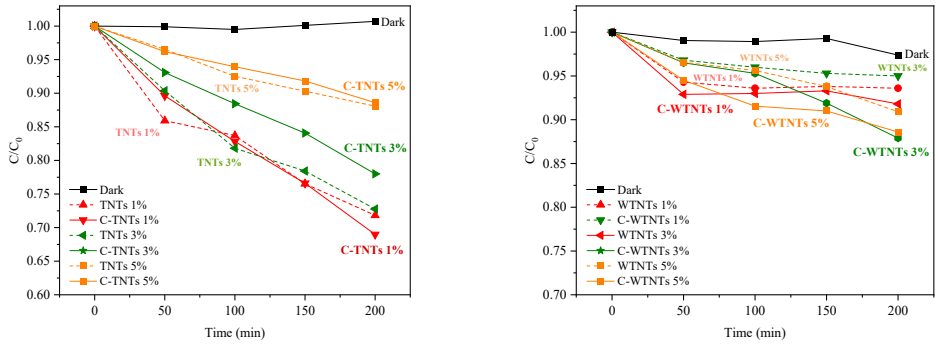

Figure 9. The degradation of MB in TNT and WTNT samples before and after coloration

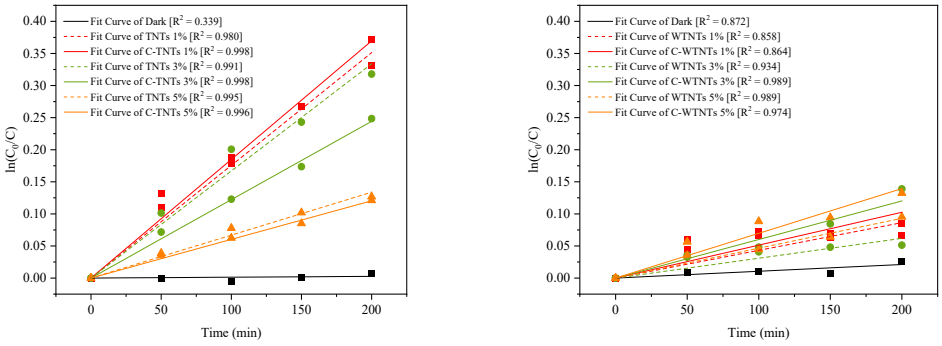

Figure 10. The relationship between degradation rate and time was analyzed to determine the k values in TNT and WTNT samples before and after coloration

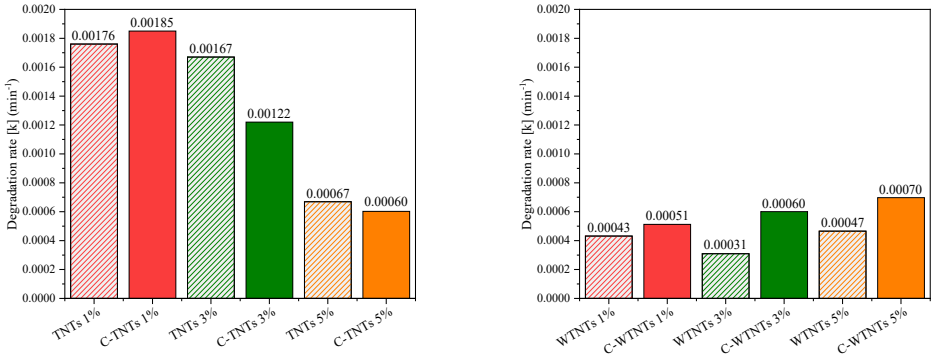

Figure 11. Comparison of the k values in TNT and WTNT samples before and after coloration

In the case of C-TNTs 1%, there was a slight increase in degradation rate compared to TNTs 1%, unlike the trends observed in C-TNTs 3 and 5%, which exhibited slower degradation than the pre-colored samples. After considering the similarities in crystal structure between the C-TNTs 1 and 3% samples, the instability of the tube morphology appears to be a significant factor. The highly distributed tube morphology plays a crucial role in charge accumulation on the film's surface, as is well known in the EC mechanism. While TNTs 1% benefit from surface porosity that enhances charge insertion, C-TNTs 1% facilitate H^+ insertion but exhibit less durability in EC devices. This means that H^+ cannot be retained in the structure for a long time, which emphasizes the importance of stability and durability in EC devices.

From this, we assume that the EC charge in C-TNTs 1% exits the structure more quickly, allowing easier contact with MB compared to the more stable C-TNTs 3%, which retains the EC charge within the structure for a longer duration. However, despite the longer retention of H^+, the C-TNTs samples still showed insufficient coloration. Additionally, the behavior of charge insertion may act like a defect, obstructing electron-hole photogeneration. Furthermore, charge insertion from the EC process on the film surface could hinder UV exposure to the longer tubes, leading to reduced direct contact with TNTs and ultimately decreasing PA efficiency.

However, during the preparation of the samples in the coloration state, we applied voltage to the films and immersed them in H_2SO_4 right before the PC testing. This might introduce slight deviations that were difficult to avoid, also creating cloudiness in the influence of EC effects on the PC behavior in both C-TNT and TNT films when compared to the C-WTNT samples.

Regarding the PA performance in WTNT samples, the deposited W layer on top of the tubes showed a significant difference in coloration state compared to TNT samples. Unfortunately, the PA performance in the pre-color state decreased. Vasilaki et al. (2017) prepared a bilayer of TiO_2/WO_3 and reported that effective exposure of the active catalyst surface to dye solution under UV irradiation facilitated both oxidation and reduction reactions, allowing photogenerated electrons and holes to reach the surface more easily, where they created hydroxyl radicals that enhanced PA performance. After considering that, in WTNT samples, the deposition of W atoms likely formed a dense layer on top of the tubes. This layer may reduce UV interaction with the main catalytic agent (TNTs). This effect was particularly noticeable in TNTs 3%, where despite wider tube diameters allowing WO_3 to penetrate inside and form a dense layer within the tubes and cover the tubes, the direct contact of TNTs with MB was probably significantly hindered, reducing the PA performance (Dozzi et al., 2016; Bogati et al., 2017)

Nevertheless, in the coloration state achieved by the EC process, all C-WTNT samples showed a clear increase in degradation efficiency, with k values increasing from 0.00043 to 0.00051 m^{-1}, 0.00031 to 0.00060 m^{-1}, and 0.00047 to 0.00070 m^{-1} for WTNTs 1, 3, and 5%, respectively. This enhancement can be attributed to the role of WO_3 layers in the EC performance, which stimulate charge insertion and form the compound H_xWO_3 (Cai et al., 2016). The effect of DI water ratios on the k values of C-WTNT samples is also influenced by the structures with high porosity and defects, which support H^+ and e^- insertion into the film structure during the EC process. However, increasing H^+ and e^- insertion in samples with high porosity resulted in decreased stability. This may explain why C-WTNTs 1 and 5% showed a trend to stabilize after 100 min, whereas C-WTNTs 3% exhibited a more consistent upward trend and indicate higher linearity.

4. Conclusions

In this research, the impact of EC on the PA performance of TNT and WTNT samples was studied, alongside the effects of DI water ratios (1, 3, and 5 wt%) in the electrolyte solution during the preparation of TNTs by anodization. It was found that increasing the DI water ratio from 1 to 3 wt% improved ion diffusion and provided stability to the nanotube morphology by enhancing both the pore diameter and the tube length. However, excessive ratios above 5 wt% caused an imbalance between the oxidation and etching processes, which tended to result in the collapse of the tube morphology and a decrement in the anatase phase of TiO_2. For WTNT samples, WO_3 films deposited on the surfaces of TNTs formed a dense layer, indicating the lower E_g values of the TNTs. The PA performance of TNT and WTNT samples, both before and after coloration via the EC process, was investigated by monitoring the degradation of MB. It was revealed that WTNT samples showed lower k values due to the WO_3 layer obstructing direct UV contact with the catalyst layer compared to TNT samples. However, in the colored state, the C-TNT samples showed a trend of reduced PA performance, while in the C-WTNT samples, the WO_3 layer played a critical role in enhancing PA performance. The k values increased from 0.00043 to 0.00051 m^{-1}, 0.00031 to 0.00060 m^{-1}, and 0.00047 to 0.00070 m^{-1} for C-WTNTs at 1, 3, and 5%, respectively. Despite the observed improvements of k values in C-WTNT samples, the PA performance remained less efficient compared to TNT and C-TNT samples. Nonetheless, this study provided possibilities for further advancements in EC properties for driving PA systems.

5. Acknowledgements

The research team would like to extend our gratitude to Thammasat University and to Assoc. Prof. Dr. Kamon Aiempanakit, our thesis advisor, for his invaluable guidance in research planning, thorough review, and correction of various shortcomings throughout the various forms of support. We would also like to thank Asst. Prof. Dr. Chantana Aiempanakit from the Division of Physics, Faculty of Science and Technology, Rajamangala University of Technology Thanyaburi, and Asst. Prof. Dr. Montri Aiempanakit from the Department of Physics, Faculty of Science, Silpakorn University, for enabling us to access their lab facilities and providing laboratory instruments to measure various research outcomes, which significantly contributed to the success of this research.

6. Conflicts of Interest

The authors declare no conflict of interest.

ORCID

Kamon Aiempanakit https://orcid.org/0000-0002-5709-5528

Montri Aiempanakit https://orcid.org/0000-0003-3162-0790

References

Alves, I., Byzynski, G., Dawson, M., & Ribeiro, C. (2017). Charge transfer mechanism of WO_3 /TiO_2 heterostructure for photoelectrochemical water splitting. *Journal of Photochemistry and Photobiology A: Chemistry*, 339, 95-102. https://doi.org/10.1016/

j.jphotochem.2017.02.024

Arvizu, M. A., Triana, C. A., Stefanov, B., Claes-Göran Granqvist, & Niklasson, G. A. (2014). Electrochromism in sputter-deposited W–Ti oxide films: Durability enhancement due to Ti. *Solar Energy Materials and Solar Cells*, 125, 184-189. https://doi.org/10.1016/j.solmat.2014.02.037

Bae, S., Shim, E., Yoon, J., & Joo, H. (2008). Enzymatic hydrogen production by light-sensitized anodized tubular TiO_2 photoanode. *Solar Energy Materials and Solar Cells*, 92(4), 402-409. https://doi.org/10.1016/j.solmat.2007.09.019

Bogati, S., Georg, A., & Graf, W. (2017). Photoelectrochromic devices based on sputtered WO_3 and TiO_2 films. *Solar Energy Materials and Solar Cells*, 163, 170-177. https://doi.org/10.1016/j.solmat.2017.01.016

Cai, G., Cui, M., Kumar, V., Darmawan, P., Wang, J., Wang, X., Eh, A. L.-S., Qian, K., & Lee, P. S. (2016). Ultra-large optical modulation of electrochromic porous WO_3 film and the local monitoring of redox activity. *Chemical Science*, 7(2), 1373-1382. https://doi.org/10.1039/c5sc03727a

Cao, L., Yuan, J., Chen, M., & Shangguan, W. (2010). Photocatalytic energy storage ability of TiO_2-WO_3 composite prepared by wet-chemical technique. *Journal of Environmental Sciences*, 22(3), 454-459. https://doi.org/10.1016/s1001-0742(09)60129-7

Chin, L. Y., Zainal, Z., Khusaimi, Z., & Ismail, S. S. (2016). Electrochemical synthesis of ordered titania nanotubes in mixture of ethylene glycol and glycerol electrolyte. *Malaysian Journal of Analytical Science*, 20(2), 373-381. https://doi.org/10.17576/mjas-2016-2002-21

Corrente, G. A., Cospito, S., Capodilupo, A. L., & Beneduci, A. (2020). Mixed-valence compounds as a new route for electrochromic devices with high coloration efficiency in the whole Vis-NIR region. *Applied Sciences*, 10 (23), Article 8372. https://doi.org/10.3390/app10238372

Dell'Edera, M., Lo Porto, C., De Pasquale, I., Petronella, F., Curri, M. L., Agostiano, A., & Comparelli, R. (2021). Photocatalytic TiO_2-based coatings for environmental applications. *Catalysis Today*, 380, 62-83. https://doi.org/10.1016/j.cattod.2021.04.023

Deshpande, R., Lee, S. H., Mahan, A. H., Parilla, P. A., Jones, K. M., Norman, A. G., To, B., Blackburn, J. L., Mitra, S., & Dillon, A. C. (2007). Optimization of crystalline tungsten oxide nanoparticles for improved electrochromic applications. *Solid State Ionics*, 178(13-14), 895-900. https://doi.org/10.1016/j.ssi.2007.03.010

Diebold, U. (2003). The surface science of titanium dioxide. *Surface Science Reports*, 48(5-8), 53-229. https://doi.org/10.1016/s0167-5729(02)00100-0

Dozzi, M. V., Marzorati, S., Longhi, M., Coduri, M., Artiglia, L., & Selli, E. (2016). Photocatalytic activity of TiO_2-WO_3 mixed oxides in relation to electron transfer efficiency. *Applied Catalysis B: Environmental*, 186, 157-165. https://doi.org/10.1016/j.apcatb.2016.01.004

El-Yazeed, W. S. A., & Ahmed, A. I. (2019). Photocatalytic activity of mesoporous WO_3/TiO_2 nanocomposites for the photodegradation of methylene blue. *Inorganic Chemistry Communications*, 105, 102-111. https://doi.org/10.1016/j.inoche.2019.04.034

Fang, H.-T., Liu, M., Wang, D.-W., Sun, T., Guan, D.-S., Li, F., Zhou, J., Sham, T.-K., & Cheng, H.-M. (2009). Comparison of the rate capability of nanostructured amorphous and anatase TiO_2 for lithium insertion using anodic TiO_2 nanotube arrays. *Nanotechnology*, 20(22), Article 225701. https://doi.org/10.1088/0957-4484/20/22/225701

Garlisi, C., Scandura, G., Yusuf, A., & Al Jitan, S. (2021). Functionalization of glass by TiO_2-based self-cleaning coatings. In F. Parrino & L. Palmisano (Eds.). *Titanium Dioxide (TiO_2) and Its Applications*, (pp. 395-428). Elsevier. https://doi.org/10.1016/b978-0-12-819960-2.00009-2

Hauch, A., Georg, A., Krašovec, U. O. & Orel, B. (2002). Comparison of

photoelectrochromic devices with different layer configurations. *Journal of the Electrochemical Society*, 149(9), Article H159. https://doi.org/10.1149/1.1496487

Her, Y.-C., & Chang, C.-C. (2014). Facile synthesis of one-dimensional crystalline/amorphous tungsten oxide core/shell heterostructures with balanced electrochromic properties. *CrystEngComm*, 16(24), 5379-5386. https://doi.org/10.1039/c4ce00430b

Huo, X., Zhang, H., Shen, W., Miao, X., Zhang, M., & Guo, M. (2019). Bifunctional aligned hexagonal/amorphous tungsten oxide core/shell nanorod arrays with enhanced electrochromic and pseudocapacitive performance. *Journal of Materials Chemistry. A,* 7(28), 16867-16875. https://doi.org/10.1039/c9ta03725j

Indira, K., Mudali, U. K., Nishimura, T., & Rajendran, N. (2015). A Review on TiO_2 nanotubes: Influence of anodization parameters, formation mechanism, properties, corrosion behavior, and biomedical applications. *Journal of Bio- and Tribo-Corrosion*, 1(4), Article 28. https://doi.org/10.1007/s40735-015-0024-x

Ivanov, S., Cheng, L., Wulfmeier, H., Albrecht, D., Fritze, H., & Bund, A. (2013). Electrochemical behavior of anodically obtained titania nanotubes in organic carbonate and ionic liquid based Li ion containing electrolytes. *Electrochimica Acta*, 104, 228-235. https://doi.org/10.1016/j.electacta.2013.04.115

Junbang, P., Aiempanakit, M., Aiempanakit, C., & Aiempanakit, K., (2024). Influences of sputtering power and the surface roughness of substrates on the microstructures of sputtered Ti films and anodized TiO_2 nanotubes. *Physica B: Condensed Matter*, 688, Article 416130. https://doi.org/10.1016/j.physb.2024.416130

Karuppasamy, A. (2015). Electrochromism and photocatalysis in dendrite structured Ti:WO_3 thin films grown by sputtering. *Applied Surface Science*, 359, 841-846. https://doi.org/10.1016/j.apsusc.2015.10.020

Karuppasamy, K. M., & Subrahmanyam, A. (2008). The electrochromic and photocatalytic properties of electron beam evaporated vanadium-doped tungsten oxide thin films. *Solar Energy Materials and Solar Cells*, 92(11), 1322-1326. https://doi.org/10.1016/j.solmat.2008.05.004

Kato, K., & Shirai, T. (2022). Highly efficient water purification by WO_3-based homo/heterojunction photocatalyst under visible light. *Journal of Alloys and Compounds*, 901, Article 163434. https://doi.org/10.1016/j.jallcom.2021.163434

Liu, Y., Jiang, S. P., & Shao, Z. (2020). Intercalation pseudocapacitance in electrochemical energy storage: recent advances in fundamental understanding and materials development. *Materials Today Advances*, 7, Article 100072. https://doi.org/10.1016/j.mtadv.2020.100072

Niklasson, G. A., & Granqvist, C. G. (2007). Electrochromics for smart windows: thin films of tungsten oxide and nickel oxide, and devices based on these. *Journal of Materials Chemistry*, 17(2), 127-156. https://doi.org/10.1039/b612174h

Ozkan, E., Lee, S.-H., Tracy, C. E., Pitts, J. R., & Deb, S. K. (2003). Comparison of electrochromic amorphous and crystalline tungsten oxide films. *Solar Energy Materials and Solar Cells*, 79(4), 439-448. https://doi.org/10.1016/s0927-0248(03)00019-9

Padmanabhan, N. T., Thomas, N., Louis, J., Mathew, D. T., Ganguly, P., John, H., & Pillai, S. C. (2021). Graphene coupled TiO_2 photocatalysts for environmental applications: A review. *Chemosphere*, 271, Article 129506. https://doi.org/10.1016/j.chemosphere.2020.129506

Reyes-Gil, K. R., Stephens, Z. D., Stavila, V., & Robinson, D. B. (2013). Composite wo_3/tio_2 nanostructures for high electrochromic activity. *ACS Applied Materials and Interfaces*, 7(4), 2202-2213. https://doi.org/10.1021/am5050696

Riyanto, E., Kristiantoro, T., Martides, E., Dedi, Prawara, B., Mulyadi, D., & Suprapto. (2023). Lithium-ion battery performance improvement using two-dimensional materials. *Materials Today: Proceedings*, 87(Part 2), 164-171. https://doi.org/10.1016/j.matpr.2023.02.392

Saharudin, K. A., Sreekantan, S., Mydin, R. B. S. N. M., Basiron, N., & Krengvirat, W. (2018). Factor affecting geometry of TiO_2 nanotube arrays (TNAs) in aqueous and organic electrolyte. In D. Yang (Ed.). *Titanium dioxide-material for a sustainable environment* (pp. 117-130). InTechOpen. https://doi.org/10.5772/intechopen.74193

Saitow, K., Wang, Y., & Takahashi, S. (2018). Mechano-synthesized orange TiO_2 shows significant photocatalysis under visible light. *Scientific Reports*, 8(1), Article 15549. https://doi.org/10.1038/s41598-018-33772-6

Sajan, C. P., Naik, A., & Girish, H. N. (2017). Hydrothermal fabrication of WO_3-modified TiO_2 crystals and their efficiency in photocatalytic degradation of FCF. *International Journal of Environmental Science and Technology*, 14(7), 1513-1524. https://doi.org/10.1007/s13762-016-1239-1

Smith, W. A., & Zhao, Y. (2008). Enhanced photocatalytic activity by aligned WO_3/TiO_2 two-layer nanorod arrays. *The Journal of Physical Chemistry C*, 112(49), 19635-19641. https://doi.org/10.1021/jp807703d

Suhadolnik, L., Marinko, Ž., Ponikvar-Svet, M., Tavčar, G., Kovač, J., & Čeh, M. (2020). Influence of anodization-electrolyte aging on the photocatalytic activity of TiO_2 nanotube arrays. *The Journal of Physical Chemistry C*, 124(7), 4073-4080. https://doi.org/10.1021/acs.jpcc.9b09522

Thakur, S., Samriti, Ojha, A., & Prakash, J. (2023). Introduction to semiconductor photocatalyst nanomaterials: properties, modifications, and multifunctional applications. In J. Prakash, J. Cho, B. C. Janegitz, & S. Sun (Eds.). *Multifunctional hybrid semiconductor photocatalyst nanomaterials* (pp. 1-30). Springer. https://doi.org/10.1007/978-3-031-39481-2_1

Thongjoon, W., Aiempanakit, K., Aiempanakit, M., & Aiempanakit, C. (2024). Influence of annealing times for W films on the structure and electrochromic properties of anodized WO_3 films. *Journal of Metals Materials and Minerals*, 34(2), Article 1969. https://doi.org/10.55713/jmmm.v34i2.1969

Vasilaki, E., Vernardou, D., Kenanakis, G., Vamvakaki, M., & Katsarakis, N. (2017). TiO_2/WO_3 photoactive bilayers in the UV–Vis light region. *Applied Physics A*, 123(4), Article 231. https://doi.org/10.1007/s00339-017-0837-1

Wahyuono, R., Ernawati, L., Maharsih, I., Widiastuti, N., & Widiyandari, H. (2019). Mesoporous WO_3/TiO_2 nanocomposites photocatalyst for rapid degradation of methylene blue in aqueous medium. *International Journal of Engineering*, 32(10), 1345-1352. https://doi.org/10.5829/ije.2019.32.10a.02

Wu, S., Sun, H., Duan, M., Mao, H., Wu, Y., Zhao, H., & Lin, B. (2023). Applications of thermochromic and electrochromic smart windows: Materials to buildings. *Cell Reports Physical Science*, 4(5), Article 101370. https://doi.org/10.1016/j.xcrp.2023.101370

Ya, H., Wang, B., Chen, F., Han, Y., Zhang, W., Wu, X., Li, R., Jiang, Q., Jia, X., & Wei, F. (2021). Electrochromic materials based on ions insertion and extraction. *Advanced Optical Materials*, 10(4), Article 2101783. https://doi.org/10.1002/adom.202101783

Yao, S., Zhang, Y., Cai, J., Hong, Y., Wang, Y., Cui, J., Shu, X., Liu, J., Tan, H. H. & Wu, Y. (2024). Construction of electrochromic porous $NiO/Ni(OH)_2$ hybrid nanoarrays with ultra-large optical modulation. *Journal of Electroanalytical Chemistry*, 954, Article 118047. https://doi.org/10.1016/j.jelechem.2024.118047

Yu, H., Chen, J., Zhang, S., Yu, Y., Wang, S., & Ye, M. (2022). Effects of electrolyte composition on the growth and properties of titanium oxide nanotubes. *Electrochemistry Communications*, 135, Article 107217. https://doi.org/10.1016/j.elecom.2022.107217

Zhang, L., Guo, J., Hao, B., & Ma, H. (2022). WO_3/TiO_2 heterojunction photocatalyst prepared by reactive magnetron sputtering for Rhodamine B dye degradation. *Optical Materials*, 133, Article 113035. https://doi.org/10.1016/j.optmat.2022.113035

Zhao, S., Wang, B., Zhu, N., Huang, Y., Wang, F., Li, R., Zhao, Y., Jiang, Q., Wu, X., & Zhang, R. (2022). Dual-band electrochromic materials for energy-saving smart windows. *Carbon Neutralization*, 2(1), 4-27. https://doi.org/10.1002/cnl2.38

Zhen, Y., Jelle, B. P., & Gao, T. (2020). *Electrochromic properties of WO_3 thin films: The role of film thickness. Analytical Science Advances*, 1(2), 124-131. https://doi.org/10.1002/ansa.202000072

Zheng, H., Ou, J. Z., Strano, M. S., Kaner, R. B., Mitchell, A., & Kalantar-zadeh, K. (2011). Nanostructured tungsten oxide - properties, synthesis, and applications. *Advanced Functional Materials*, 21(12), 2175-2196. https://doi.org/10.1002/adfm.201002477

Zhou, X., Huang, E., Zhang, R., Xiang, H., Zhong, W., & Xu, B. (2023). Multicolor tunable electrochromic materials based on the Burstein–Moss effect. *Nanomaterials*, 13(10), Article 1580. https://doi.org/10.3390/nano13101580

Zhou, H., Wang, H., Yue, C., He, L., Li, H., Zhang, H., Yang, S., & Ma, T. (2024). Photocatalytic degradation by TiO_2-conjugated/coordination polymer heterojunction: Preparation, mechanisms, and prospects. *Applied Catalysis B: Environment and Energy*, 344, Article 123605. https://doi.org/10.1016/j.apcatb.2023.123605